https://doi.org/10.5194/egusphere-2022-1008
Preprint. Discussion started: 10 October 2022
© Author(s) 2022. CC BY 4.0 License.

The contrasted phytoplankton dynamics across a frontal system in the southwestern Mediterranean Sea.

Roxane Tzortzis[1], Andrea M. Doglioli[1], Stéphanie Barrillon[1], Anne A. Petrenko[1], Lloyd Izard[2], Yuan Zhao[3], Francesco d'Ovidio[2], Franck Dumas[4], and Gérald Gregori[1]

[1]Aix Marseille Univ., Université de Toulon, CNRS, IRD, MIO UM 110, 13288, Marseille, France
[2]Sorbonne Université, CNRS, IRD, MNHN, Laboratoire d'Océanographie et du Climat: Expérimentations et Approches Numériques (LOCEAN-IPSL), Paris, France
[3]CAS Key Laboratory of Marine Ecology and Environmental Sciences, Institute of Oceanology, Chinese Academy of Sciences, Qingdao, People's Republic of China
[4]SHOM, Service Hydrographique et Océanographique de la Marine, 13 rue de Chatellier, CS592803, 29228 Brest, CEDEX 2, France

Correspondence: Roxane TZORTZIS (roxane.tzortzis@mio.osupytheas.fr)

Abstract.

Phytoplankton plays a major role in the ocean, being the basis of the marine food web and controlling the biogeochemical cycles. Numerical simulation have shown that finescale structures such as fronts are often suitable places for the generation of vertical velocities, transporting subsurface nutrients to the euphotic zone and thus modulating phytoplankton abundance and community structure. Since several years, observations have concentrated on nutrient fluxes along these structures. Instead, direct in situ estimations of the phytoplankton growth rates are much less numerous ; although difficult to obtain, they provide a precious information on the ecosystem functioning. Here, we consider the case of a front separating two water masses characterized by several phytoplankton groups with different abundances, in the southwestern Mediterranean Sea. In order to estimate possible differences in growing rates, we used an adaptive and Lagrangian sampling strategy to measure the phytoplankton diurnal cycle in these two water masses. The use of a size-structured population model was then applied to these data to estimate the growth and division rates for each phytoplankton groups identified by flow cytometry, showing that these two population parameters are significantly different on the two sides of the front, and consistent with the relative abundances. Our results introduce a general method for estimating growth rates at frontal systems, paving the way to in situ exploration of finescale biophysical scenarios.

1 Introduction

Phytoplankton is essential for the functioning of the oceans and for the marine ecosystems. Its capacity to perform photosynthesis influences the global carbon cycle, by fixing CO_2 and exporting it either into the ocean depth or to the higher trophic layers through the biological pump (Field et al., 1998; De La Rocha and Passow, 2007). That is why it is primordial to understand the factors that rule its abundance and diversity, particularly in the actual context of climate change (Bates et al., 2018).

https://doi.org/10.5194/egusphere-2022-1008
Preprint. Discussion started: 10 October 2022
© Author(s) 2022. CC BY 4.0 License.

Numerical simulations and remote sensing observations have demonstrated that finescale, i.e. ocean structures characterized by horizontal scale of the order of 1–100 km, with a short lifetime (days–weeks) can play a key role in phytoplankton biological processes. Indeed, the phytoplankton temporal scale is of the same order of magnitude as the one of finescale processes such as eddies, filaments or fronts, suggesting the possibility of a close coupling between phytoplankton growth and finescale forcing. Previous studies have established that finescale frontal structures could induce vertical velocities (Rudnick, 1996), which could modulate the light availability (a change in depth induces a change in irradiance) and drive nutrients in the euphotic layer, thus impacting the abundance and the distribution of phytoplankton communities (e.g. Clayton et al., 2014; Pidcock et al., 2016; Mahadevan, 2016; Lévy et al., 2018). However, most of these works have focus on the estimation of nutrient fluxes and much less is known about the phytoplankton dynamic across these frontal area. This is due to the rapid evolution of phytoplankton communities across these ephemeral finescale structures, that makes them particularly difficult to sample in situ with classical methods of observation. That is why, new sampling strategies were required to track these finescale structures. Some recent cruises have used remote sensing and numerical simulations to define the sampling strategy allowing to target and measure finescale features with physical sensors at high frequency (Shcherbina et al., 2015; Pascual et al., 2017; Petrenko et al., 2017). Concerning the biological variables, although some progress in the understanding of phytoplankton cell cycle has been provided thanks to incubation or sample manipulation (Worden and Binder, 2003), these conventional methods cannot be easily conducted at a daily frequency. A solution is to perform in situ measurements at high frequency (every 20 min) and resolution (1–10 km), thanks to automated analytical flow cytometry, in order to resolve these biological processes at time scales relevant to the cells responses to their environment (Thyssen et al., 2008; Fontana et al., 2018).

The PROTEVSMED-SWOT cruise was performed in the southwestern Mediterranean Sea, south of the Balearic Islands (Dumas, 2018; Garreau et al., 2020) with the aim to study the physical and biological coupling at finescale, adopting a Lagrangian adaptive sampling strategy. This approach consists in using remote sensing products (such as sea surface salinity (SSS), temperature (SST), chlorophyll a concentration ([chla]) and altimetry) to determine the position of oceanic features and guide in quasi-real time the route of the ship and the sampling strategy across these structures of interest. Thanks to this strategy it was possible to identify a moderately energetic front separating two distinct water masses and to highlight its influence on the distribution of the phytoplankton abundances (Tzortzis et al., 2021). As these two water masses had a signature in temperature and salinity, Tzortzis et al. (2021) identified two types of Atlantic Water (AW) at different stage of mixing, separated by the front. The first AW located South of the front, characterized by absolute salinity (S_A) between 37 $\mathrm{g\,kg^{-1}}$ and 37.5 $\mathrm{g\,kg^{-1}}$ is named "younger AW" and corresponds to AW more recently entered into the Mediterranean Sea. Whereas the second AW, referred as "older AW", is found North of the front, and is characterized by a higher S_A (37.5 $\mathrm{g\,kg^{-1}}$ to 38 $\mathrm{g\,kg^{-1}}$). Contrasted phytoplankton abundances were observed in these two water masses, with the smallest phytoplankton such as *Synechococcus* dominating south of the front.

This study constitutes an important improvement in the understanding of the role of frontal structures at finescale on phytoplankton distribution. Nevertheless, open questions remain concerning the mechanisms generating the observed distribution. Is it exclusively driven by the dynamics of the ocean currents ? What is the role of biological processes ? In the present study, we attempt to explain the particular patterns of phytoplankton abundances observed by automated flow cytometry during the

https://doi.org/10.5194/egusphere-2022-1008
Preprint. Discussion started: 10 October 2022
© Author(s) 2022. CC BY 4.0 License.

PROTEVSMED-SWOT in the frontal structure, using the size-structured population model of Sosik et al. (2003). This model is based on the reconstruction of the diurnal cycle of phytoplankton: during daylight, active individual cells increase in volume due to photosynthesis. The model follows the cells size distribution, and determines the growth and division rates, for a specific functional group determined by flow cytometry (Sosik et al., 2003; Marrec et al., 2018). Several studies have already used this model, but most of them applied it only to *Synechococcus* or *Prochlorococcus* (Ribalet et al., 2010; Hunter-Cevera et al., 2014; Marrec et al., 2018). An originality of our work is the attempt to apply this model also on the various phytoplankton functional groups identified by flow cytometry. Our approach implies that, except for *Synechococcus* which refer to a taxonomic group (*cyanobacteria*), other flow cytometric groups refer to different range of sizes (estimated from light scatter) and fluorescence intensities related to their photosynthetic pigment content. An other originality of our study is that, to our knowledge, our work is one of the first to apply the model of Sosik et al. (2003) in a context of a Lagrangian sampling strategy to follow two contrasted water masses separated by a front and to study the temporal evolution of their respective phytoplankton communities and dynamics.

2 Materials and methods

2.1 The sampling strategy

The PROTEVSMED-SWOT cruise, dedicated to the study of finescale dynamics, has been conducted in the south of the Balearic Island between April 30th and May 18th 2018, on board of the RV *Beautemps-Beaupré* (Fig. 1a). This site has been chosen in the scope of the future altimetric satellite SWOT (Surface Water Ocean Topography) will launch in 2023. This region has the advantage of being at the cross-over of two tracks of the satellite during the so called fast-sampling-phase dedicated to test and calval of the satellite (https://www.swot-adac.org, last access: September 27, 2022). Furthermore, the Mediterranean sea is a high biodiversity hot spot associated to conditions of oligotrophy and moderate energy, unlike oceanic areas as western boundary currents or eastern boundary upwellings that are largely explored and where the intense dynamics or the large nutrient input can mask the finescale coupled dynamics. The PROTEVSMED-SWOT cruise followed an adaptive and Lagrangian strategy, measuring at high resolution several physical and biological variables with in situ sensors installed both on board (Acoustic Doppler Current Profiler (ADCP), thermosalinograph (TSG), flow cytometer installed on the seawater supply of the TSG) and on a towed vehicle (Seasoar). Tzortzis et al. (2021) provides the detailed description of all the in situ measurements performed during the cruise. In the present study, as we focus on the biological aspects in two contrasted water masses separated by a front, the following description is focused on the sampling strategy as well as the measurements performed by the TSG and the flow cytometer.

Our sampling strategy was both adaptive and Lagrangian, meaning that the vessel route was designed ad-hoc on the basis of daily remote sensing dataset of altimetry-derived currents and ocean color observations to follow and sample the same water masses for some days. In particular, maps of [chla] derived from satellite data allowed to identify two water masses, characterized by distinct [chla] values and separated by a zonal front at about 38° 30' N (Fig. 1b). This front has also been detected using the in situ horizontal velocities, temperature and salinity, as described by Tzortzis et al. (2021). Once the front

https://doi.org/10.5194/egusphere-2022-1008
Preprint. Discussion started: 10 October 2022
© Author(s) 2022. CC BY 4.0 License.

localized, repeated transects were performed across the two water masses separated by the front adapting the temporal sampling to the biological time scales in order to reconstruct the phytoplankton 24-hours diurnal cycle for each water mass (Fig. 1c).

2.2 In situ measurements

The sea surface temperature and salinity have been measured by a thermosalinograph (TSG) SeaBird Electronics (SBE) 45, which is an underway sensor able to continuously pump seawater at 3 m (more details about the TSG sensor in Tzortzis et al. (2021)). These two physical variables have been converted into conservative temperature (Θ) and absolute salinity (S_A) using the TEOS-10 standards of McDougall et al. (2012). To sample at high frequency the phytoplankton cells, an automated CytoSense flow cytometer (CytoBuoy b.v.) was installed on board and connected to the seawater circuit of the TSG. A sheath fluid made of 0.1 $\mu\mathrm{m}$ filtered seawater stretched the sample in order to separate, align, center and drive the individual particles (i.e. cells) through a laser beam (488 nm wavelength). Several optical signals were recorded when each particle crosses the laser beam: the forward angle light scatter (FWS) and 90° side-ward angle scatter (SWS), related to the size and the structure (granularity) of the particles. Two distinct fluorescence emissions induced by the light excitation were also recorded, a red fluorescence (FLR) induced by chlorophyll a content and an orange fluorescence (FLO) induced by the phycoerythrin pigment content.

The CytoUSB software (Cytobuoy b.v.) was used to configure and control the flow cytometer and set two distinct protocols, running sequentially every 30 min. A total of 1164 samples was analysed during the cruise. The first protocol (FLR6) was dedicated to the analysis of the smaller phytoplankton, thanks to a FLR trigger threshold fixed at 6 mV, and a volume analysed set up at 1.5 cm^3. The second protocol (FLR25) targeted nanophytoplankton and microphytoplankton with a FLR trigger level fixed at 25 mV and an analyzed volume of 4 cm^3. Data were stored in real time on a computer. Once recorded, they were analyzed with the CytoClus software (Cytobuoy b.v.) which retrieves information from the 4 pulse shapes curves (FWS, SWS, FLO, FLR) obtained for every single cell. These curves were then projected into distinct two-dimensional planes (cytograms) by computing the curves integral. Using a combination of various cytograms (e.g., FWS vs. FLR, FLO vs. FLR) allows to determine optimal clusters of cells sharing similar properties. These clusters have been demonstrated in the literature as Phytoplankton functional groups (PFGs) (Dubelaar and Jonker, 2000; Reynolds, 2006; Thyssen et al., 2008; Edwards et al., 2015). The PFGs abundance (cells per cubic centimetre) and average variable intensities are extracted from each sample. Finally, the information on each PFG is fetched in the appropriate protocol (e.g., nanophytoplankton in FLR25), resulting in 582 samples (1164/2). Considering the successive samples acquisition permit to monitor the PFGs dynamics over time and space (Thyssen et al., 2008). The irradiance (wavelengths between 400 and 1000 nm) was also measured during the cruise by a CMP6 pyranometer (Kipp and Zonen; https://www.campbellsci.fr/cmp6, last access: September 27, 2022).

2.3 The size-structured population model

The size-structured population model described in Sosik et al. (2003) and adapted by Dugenne et al. (2014) was used to estimate the phytoplankton growth and division rates of phytoplankton in situ. The cell cycle of phytoplankton alternates between cellular growth during the interphase and division at the end of the mitosis. That is why the phytoplankton cells transit in dif-

https://doi.org/10.5194/egusphere-2022-1008
Preprint. Discussion started: 10 October 2022
© Author(s) 2022. CC BY 4.0 License.

ferent size classes following a circadian clock. The size-structured population model is based on this size classes distribution. It stands on the assumptions that (i) cell growth is determined by light exposure, (ii) the probability of a cell dividing depends on its size, (iii) all cells have the same probability to change to another size class, and (iv) a cell divides into two daughter cells, each half the size of the mother cell.

To use the model, the light scatter signal recorded for each cell by the flow cytometer must be converted in a size (length) and then in a biovolume (v), using a power law relationship between cell size and FWS (Sosik et al., 2003). The absolute number of cells (**N**) and proportions of cells in the various size classes (**w**) were investigated during a 24 h period to follow the transitions of cells in each size class for the m size classes defined in our study. The temporal transitions between size classes are assumed to result from either cellular growth, supported by photosynthetic carbon assimilation, or asexual division (i.e., mitosis). The number of classes m was chosen in order to cover the entire observed biovolume from v_{min} to v_{max} Eq. (1).

$$\mathbf{w} = \frac{\mathbf{N}}{\sum_{i=1}^{m} N_{i|v=v_i}} \tag{1}$$

with $v_{1,2,\ldots,i,\ldots m}$ denoting the size classes.

The increase in cell size occurring during the interphase is dependent of the proportion of cells that will grow between t and $t + dt$, noted $\gamma(t)$. This probability is expressed as an asymptotic function depending only on the light intensity necessary to the photosynthesis Eq. (2):

$$\gamma(t) = \gamma_{max} \cdot (1 - e^{-E(t)/E^*}) \tag{2}$$

with E the irradiance (i.e., the light intensity measured by the pyranometer), E^* the irradiance scaling parameter, and γ_{max} the maximal proportion of cells growing between t and $t + dt$.

However, the decrease of cell size depends on the proportions of cells that will enter mitosis between t and $t + dt$. Indeed, during mitosis, the division of one mother cell generates two daughter cells half the size their mother cell. The proportion of cells entering mitosis is expressed as a function of both time and cell size Eq. (3).

$$\delta(t) = \delta_{max} f(\mu_v {\sigma_v}^2) f(\mu_t {\sigma_t}^2) \tag{3}$$

with f the normal probability density, v the cell biovolume, δ_{max} the maximal proportion of cells entering mitosis, μ_v the mean of the size density distribution, σ_v the standard deviation (SD) of the size density distribution, μ_t the mean of the temporal density distribution, and σ_t the SD of the temporal density distribution. Note that the decrease of cell size controls the population net growth rates Eq. (4).

$$\mu(t) = \frac{1}{dt} \cdot ln(1 + \delta(t)) \tag{4}$$

https://doi.org/10.5194/egusphere-2022-1008
Preprint. Discussion started: 10 October 2022
© Author(s) 2022. CC BY 4.0 License.

The initial distribution of the cell size, $\mathbf{N}(0)$, is projected with a time step dt = 10/60 h, to construct the normalized size distribution, $\mathbf{w}(t)$, over a 24 h period Eq. (5), with ˆ standing for model predictions.

$$\hat{\mathbf{N}}(t+dt) = A(t)\hat{\mathbf{N}}(t) \qquad and \qquad \hat{\mathbf{w}}(t+dt) = \frac{A(t)\hat{\mathbf{N}}(t)}{\sum A(t)\hat{\mathbf{N}}(t)} \tag{5}$$

The tridiagonal transition matrix, $\boldsymbol{A}(t)$, contains:

1. the stasis probability, expressed as the proportions of cells that neither grew nor divided between t and $t+dt$ (Sosik et al., 2003),
2. the growth probability (γ), expressed as the proportions of cells that grew between t and $t+dt$,
3. the division probability (σ), expressed as the proportions of cells that entered division between t and $t+dt$.

Depending on the set of optimal parameters (Table 1), the function $\boldsymbol{\theta}$ Eq. (6) minimizes the Gaussian error distribution between predictions ($\hat{\mathbf{w}}$) and observations ($\mathbf{w}$). Their standard deviations are estimated by a Markov chain Monte Carlo approach that samples $\boldsymbol{\theta}$ from their prior density distribution, obtained after running 200 optimizations on bootstrapped residuals.

$$\boldsymbol{\theta} = \{\gamma_{max}, E^*, \delta_{max}, \mu_v, \sigma_v, \mu_t, \sigma_t\} = argmin(\sum(\boldsymbol{\theta})) \tag{6}$$

with γ_{max} and δ_{max} the proportions of cells in growing phase and in mitosis, respectively, E^* the irradiance scaling parameter, μ_v and σ_v the mean and the SD of size density distribution, μ_t and σ_t the mean and the SD of temporal density distribution (cf Table 1).

$$\sum(\boldsymbol{\theta}) = \sum_{t=T0}^{T1day} \sum_{i=1}^{m} (\mathbf{w} - \hat{\mathbf{w}}(\boldsymbol{\theta}))^2 \tag{7}$$

Ultimately, the equivalent of the temporal projection of proportions is conducted on the absolute diel size distribution ($\mathbf{N}$) with the optimal set of parameters to estimate population intrinsic growth rates (μ_{size}) on a 24 h period, from which the hourly logarithmic difference of observed abundances is subtracted to obtain the daily average population loss rates ($\bar{l}$) Eq. (8).

$$\mu_{size} = \frac{1}{24 \cdot \frac{1}{dt} + 1} ln(\frac{\hat{\mathbf{N}}(T_{1day})}{\mathbf{N}_{T_0}}) \qquad and \qquad \bar{l} = \int^{dt=1h} \mu_{size}(dt) - \frac{1}{dt} \cdot ln(\frac{\mathbf{N}(t+dt)}{\mathbf{N}(t)}) \tag{8}$$

Since the model allows for any cell to grow, divide or be at equilibrium over the entire integration period (asynchronous populations), the growth rates μ_{size} superior to the median size ratio $\mu_{ratio} = ln(v_{max}/v_{min})$ (indicative of a synchronous population) are assumed to be well represented.

https://doi.org/10.5194/egusphere-2022-1008
Preprint. Discussion started: 10 October 2022
© Author(s) 2022. CC BY 4.0 License.

3 Results

3.1 Identification of the phytoplankton functional groups by flow cytometry

Up to 9 groups of phytoplankton have been identified on the cytograms (Fig. 2), thanks to their light scatter (forward scatter FWS, and sideward scatter SWS) and fluorescence intensities (red fluorescence FLR, and orange fluorescence FLO). These groups have been called using the conventional names used by flow cytometrists, i.e., some groups relate to taxonomy (*Synechococcus*, Cryptophytes) while others relate to a range of sizes (picoeukaryotes, nanoeukaryotes) as described by Sieburth et al. (1978). *Synechococcus* (Syn on Fig. 2c) is a prokaryotic picophytoplankton that can be distinguished from the other picophytoplankton owing to its high FLO intensity, induced by phycoerythrin pigment content. Cryptophytes (Crypto on Fig. 2c) were also discriminated from the other groups as they also produce a characteristic orange fluorescence induced by phycoerythrin. Concerning the other phytoplankton groups, 4 eukaryotic picophytoplankton groups were put in evidence: Pico1 (on Fig. 2c) characterized by lower FLR and FLO intensities than *Synechococcus*, Pico2 and Pico3 (on Fig. 2d) with higher FWS, SWS and FLR intensities than Pico1, PicoHFLR (on Fig. 2a) has a high FLR signal induced by chla. We defined 2 distinct nanophytoplankton groups (SNano and RNano) according to their high FLR and FLO intensities. SNano exhibits higher SWS/FWS ratio and SWS intensities than RNano (Fig. 2b and Fig. 2a). Finally, microphytoplankton (Micro) is characterized by the highest FLR and FWS intensities (Fig. 2c).

3.2 Spatio-temporal distribution of phytoplankton abundances in the two water masses

The sampling strategy adopted during PROTEVSMED-SWOT enabled us to sample two water masses with different properties. The map of the satellited-derived surface [chla] shows higher concentration in the Northern part of the sampling route, corresponding to older AW, than in the the Southern part, corresponding to younger AW (Fig. 1b). Figure 3 shows the properties of the sea surface water as a function of time (from 11 May 00:00 to 13 May 12:00 UTC) along the sampling route. The older AW is characterized by a colder temperature and higher values of salinity than the younger AW. Figure 3 also displays the abundances of each phytoplankton group over these two water masses. *Synechococcus* and Pico2 are the most abundant. They present a clear surface distribution pattern, with high abundances in the warm and low salinity water, corresponding to the young AW. A similar distribution is observed for Pico1, Pico3 and RNano but with lower abundances than *Synechococcus* and Pico2. The abundances of SNano, PicoHFLR and Cryptophyte show less contrasts along the cruise than the previous groups, nonetheless the highest abundances can be distinguished in the younger AW, in particular in the second and third passage (transect) across this water mass. Finally, microphytoplankton is the less abundant group, but it clearly shows a contrast between the two water masses, opposite to the one of the other phytoplankton groups.

3.3 Phytoplankton cellular growth and division in the two water masses

In addition to the cell abundances measured along the route of the ship, the phytoplankton diurnal cycle in the two water masses was also reconstructed using the size-structured population model (Sosik et al., 2003) to address the phytoplankton

https://doi.org/10.5194/egusphere-2022-1008
Preprint. Discussion started: 10 October 2022
© Author(s) 2022. CC BY 4.0 License.

dynamics. We talk about reconstruction because the ship did not spend 24 h in a row in each water mass but sailed along two routes, each forming a sort of racetrack passing alternately through the two water masses. This adaptive Lagrangian approach allows sampling of the different functional groups of phytoplankton in each water mass (Fig. 1b). By eliminating the dates and keeping the associated sampling times (Fig. 1c), the 24-hour nocturnal cycle can be reconstructed for each water body. That relies on the hypothesis that the phytoplankton community and dynamics are the same on the two days, and that hydrology and physics for each water mass remain alike during sampling. Figures 4, 5, 6 show the phytoplankton biovolume distribution over 24 h for *Synechococcus*, RNano and SNano respectively. We have also reconstructed the 24-hour irradiance in the two water masses represented by the red lines on Fig. 4, 5, 6. Indeed, one of the most important parameters of this model is irradiance, since cell growth is dependent on light exposure due to photosynthesis. The reconstruction of the circadian cycle shows that irradiance (i.e., the area under the curves on Fig. 4, 5 and 6) is almost the same in the two water masses, and the computation of irradiance with a trapezoidal integration give intensities of 286 and 299 $\mu E\,m^{-2}\,s^{-1}$ for the older AW and the younger AW, respectively (Fig. A1).

Furthermore, the comparison between the biovolume observed in situ and the biovolume predicted by the model is sound and confirms that the model-predicted cell size distributions well recapitulated the diurnal cycle reflecting either growth or cell division. From the biovolume predicted it is possible to derive a specific growth rate (μ_{size}) and a loss rate (l) for both populations in the two water masses. Table 2 summarizes the growth and loss rates found for the different phytoplankton groups in the two water masses. For *Synechococcus*, the older AW is populated by larger cells (mean biovolume v_{mean} = 0.38 μm^3) than in the younger AW, (mean biovolume v_{mean} = 0.21 μm^3). Furthermore, in the older AW, the large cells of *Synechococcus* have a growth rate μ_{size} = 0.25 d^{-1} and a loss rate l = -0.64 d^{-1}, whereas in younger AW the smaller cells are characterized by a high growth rate (μ_{size} = 0.71 d^{-1}) and a low division rate (l = -0.21 d^{-1}). Concerning RNano, the cell size distribution between the older AW (Fig. 5a,c) and the younger AW (Fig 5b,d) is less contrasted than for *Synechococcus* (Fig. 4). Indeed, we cannot observe a significant difference between the biovolumes, which are equal to 61.9 μm^3 and 59.3 μm^3 in the older AW and in the younger AW respectively. Furthermore, compared to *Synechococcus*, the RNano growth rates are generally low (Table 2), but with a contrast between the two water masses. Indeed, the growth rate is higher in the younger AW (μ_{size} = 0.04 d^{-1}) than in the older AW (μ_{size} = 0.01 d^{-1}). However, the loss rates of RNano are high, especially in the younger AW (l = -1.32 d^{-1}) in comparison to the older AW (l = -0.87 d^{-1}). The size distribution of SNano is similar to those of the other phytoplankton described previously. Indeed, the older AW is predominantly composed of large SNano cells (v_{mean} = 84.8 μm^3), compared to the younger AW (v_{mean} = 60.6 μm^3). Furthermore, the highest values of SNano biovolume and loss rate are found in the older AW, as observed for RNano.

4 Discussion

4.1 The phytoplankton diurnal cycle

Although it has been clearly demonstrated that phytoplankton plays a fundamental role in the ocean ecosystem functioning, numerous questions remain open about their population dynamics in relation with the finescale structures.

https://doi.org/10.5194/egusphere-2022-1008
Preprint. Discussion started: 10 October 2022
© Author(s) 2022. CC BY 4.0 License.

Coupling high-resolution in-situ flow cytometry measurements performed with an adaptive and Lagrangian sampling strategy, with the size-structured population model developed by Sosik et al. (2003) allowed us to characterize the structure of phytoplankton and to reconstruct the diurnal cycle during which cell growth and division alternate over a 24 h period in two contrasted water masses separated by a finescale front. The values of growth rates (μ_{size}) and loss rates (l) found for *Synechococcus* in our study are of the same order of magnitude as the results of Marrec et al. (2018), who also applied the size-structured model of Sosik et al. (2003) in the northwestern Mediterranean Sea. In section 3.3, we have shown that the largest cells of *Synechococcus* are dominant in the older AW. These *Synechococcus* cells are characterized by a larger range of biovolume, a lower growth rate and a higher loss rate than those located in the younger AW (Table 2). This is due to the fact that the older AW is composed of *Synechococcus* cells transiting in all the cell cycle stages all day long (Fig. 4a, c). The cells are in average larger than in the younger AW as they grow slower at the population scale (lower growth rate). Conversely, in the younger AW the distribution of the *Synechococcus* biovolume is narrower, which could be explained by cells more active, more homogeneous in terms of size (biovolume) and better synchronized, leading to a smaller spread of the cell biovolume (Fig. 4b,d) with a dominance of *Synechococcus* small cells (Fig. 3). That explains why the patchiness of *Synechococcus* size distribution in the older AW (Fig. 4a, c) is more extensive than in the younger AW, where the size distribution is narrower (Fig. 4b, d). That also explains why higher abundances of *Synechococcus* are found in the younger AW (Fig. 3).

The patchiness of size distribution of RNano and SNano (Fig. 5 and 6) is similar to those of *Synechococcus* (Fig. 4), with more extensive distribution located in the older AW, especially for SNano. As for *Synechococcus*, the nanophytoplankton patchiness could explain the distribution in terms of abundances in the two water masses (Fig. 3).

We have also modeled the diurnal cycle for the picophytoplankton groups i.e., Pico1, Pico2, Pico3, PicoHFLR, (cf Fig. 2). However, we obtained very noisy size distributions and couldn't obtain a valid measurement, hence these distributions are not considered further in this study. A possible explanation is that picophytoplankton is often characterized by an important biodiversity (Siokou-Frangou et al., 2010) with potentially different dynamics. Indeed, except for *Synechococcus* and Cryptophytes which are taxonomic groups, the other phytoplankton groups are ataxonomic and defined only based on their size class estimated by the light scattering measured by the flow cytometer. These populations are gated out based on the expertise of the flow cytometrists. Obviously, additional analysis such as metabarcoding should have been done to address the biodiversity and test this hypothesis, but as the samples were analysed online, no sample was brought back to the laboratory to perform further investigation. On the contrary, a clear pattern was found for the nanophytoplankton group probably because the nanophytoplankton is mostly dominated by diatoms in the Mediterranean Sea (Siokou-Frangou et al., 2010), especially in frontal systems (Claustre et al., 1994). Finally, as microphytoplankton and Cryptophytes were not abundant enough to allow a reliable determination of their abundances and cell cycles, they were not considered in this study.

4.2 The influence of the frontal system on the phytoplankton dynamics

Oceanic finescales (typically 1-100 km) have relatively short lifetimes from days to weeks. However, due to the strong gradients created by their energetic dynamics they critically affect both ocean physics and ecology. These gradients are associated with strong vertical velocities at the origin of a vertical transport connecting the ocean's upper layer to its interior. Furthermore,

https://doi.org/10.5194/egusphere-2022-1008
Preprint. Discussion started: 10 October 2022
© Author(s) 2022. CC BY 4.0 License.

the temporal scale associated with this dynamics (both horizontal and vertical) is in the same order of magnitude than many important oceanic processes including biogeochemical cycles and biodiversity. This suggests the possibility of a close coupling between the finescale forcing and the phytoplankton distribution and growth. In our previous article Tzortzis et al. (2021) provided a description of the hydrodynamics and the hydrology in the same of the area of the present of the region South of the Balearic Islands corresponding to a cross-over of the next SWOT satellite (Fig. 1). In the following, we attempt to establish the potential link between these different physical forcings and the particular distribution of phytoplankton in terms of cells size and abundances. Figure 7 summarizes the physical forcing evidenced in this area in the previous publication during the PROTEVSMED-SWOT cruise, superimposed with the biovolumes and the abundances of the different phytoplankton groups sampled in situ by the automated flow cytometer.

Physical hydrodynamics and, in particular, vertical velocities play a key role on phytoplankton dynamics as vertical velocities modulate nutrients availability and irradiance of phytoplankton (intensity and quality vary with depth), two essential variables for phytoplankton growth (Lévy et al., 2001; Pidcock et al., 2016; Mahadevan, 2016). The computation of the vertical motions in the frontal area, as represented in Fig. 7 (see also Fig. A2), show that in the frontal area upwellings and downwellings occur with different intensities. Indeed, the area north of the front, corresponding to the older AW, is characterized by a more intense upwelling than the younger AW south of the front. That could explain the special distribution of phytoplankton size classes and abundances in the two water masses, observed during our cruise. Indeed, the older AW is characterized by larger cells of *Synechococcus* and nanophytoplankton with low abundances, whereas the younger AW is dominated by small cells with high abundances. Furthermore, microphytoplankton (i.e., high phytoplankton size) is more abundant in older AW than in the younger AW. Previous studies have shown that picophytoplankton are more abundant in oligotrophic regions (Zhang et al., 2008; Cerino et al., 2012). Indeed, their better surface:size ratio due to their small size confers them a better capacity to inhabit areas with very low nutrient concentration compared to larger phytoplankton (Kiørboe, 1993; Marañón, 2015, e.g.,). As far as nutrients are concerned, Bethoux (1989) and Schroeder et al. (2010) have observed that the older AW is more enriched with nutrients than the younger AW because during its circulation across the Mediterranean basin, the older AW receives nutrient inputs from continent (river discharges, rain, wind). If in our study we do not have nutrient data, we can suppose that the nutrient distribution across the two water masses should be similar to the one measured during the previous studies of Bethoux (1989) and Schroeder et al. (2010). In addition, the distribution of phytoplankton cells size and abundances in the two water masses is in agreement with the study of Jacquet et al. (2010) and Mena et al. (2016) in the Alboran Sea and in the southern part of the Balearic Island, respectively. They also found the highest abundances of the small phytoplankton (*Synechococcus* and picophytoplankton) in the most oligotrophic waters, i.e., the younger AW. Some studies have attempted to highlight a link between hydrological condition and the phytoplankton dynamic (Qasim et al., 1972; Marañón et al., 2012, e.g.,). However, their results showed that the influence of these hydrological parameters on the phytoplankton growth and distribution was difficult to estimate, compared to the effects of nutrient availability and radiation exposure.

https://doi.org/10.5194/egusphere-2022-1008
Preprint. Discussion started: 10 October 2022
© Author(s) 2022. CC BY 4.0 License.

5 Conclusion and perspectives

Phytoplankton structure and dynamics are a complex result of many interacting biological and physical phenomena. Biological processes can be either intrinsic, such as cell growth, or extrinsic such as cell death by viral lysis or grazing. Physical forcings in particular at finescales are also important, because they can influence the nutrient and irradiance, both parameters being fundamental for primary production by photosynthesis.

In this study, we have focused on a frontal structure separating two distinct water masses both in terms of hydrology and phytoplankton abundances. The reconstruction of the diurnal cycle for several phytoplankton groups in these two water masses, under the influence of physical conditions met in situ provides a better understanding of the particular distribution of the phytoplankton groups in this area. The estimates of specific growth rates for the various phytoplankton groups is a key to better understand and quantify their respective biogeochemical and ecological contributions in oligotrophic ecosystems, where they play a major role. Furthermore, direct integration of growth rates in biogeochemical models (Cullen et al., 1993) should be taken into account for a better assessment of the biogeochemical contribution of phytoplankton in oligotrophic ecosystems and to better forecast its evolution in the context of global change.

This work paves the way for the future cruise which will provide a unique opportunity for a more detailed study of physical–biological finescale coupling. Indeed, we plan future experiments again in the South western Mediterranean in spring 2023, after the launch of the SWOT satellite which will provide high resolution altimetry-derived current. Involving high-resolution nutrient measurements (and also high-precision ones, considering the oligotrophy of the Mediterranean Sea), coupled with metabarcoding (to address the biodiversity of phytoplankton), zooplankton and virus sampling, we will improve the understanding of zooplankton grazing and viral lysis on the different phytoplankton groups. Furthermore, we aim to explore how biogeochemical and ecological role of the finescales in regions of weak circulation are different from the ones more documented in highly energetic regions like boundary currents. In the Mediterranean sea, the low nutrient content is indeed the perfect condition when addressing this question, because even weak horizontal or vertical nutrient redistributions associated with the finescale circulation are likely to result in a biological response (Talmy et al., 2014; Hashihama et al., 2021).

Data availability. The data are open access and available at https://www.seanoe.org/data/00512/62352/ (last access: September 27, 2022) (Dumas, 2018).

https://doi.org/10.5194/egusphere-2022-1008
Preprint. Discussion started: 10 October 2022
© Author(s) 2022. CC BY 4.0 License.

Author contributions. RT post-processed the in situ observations, performed the analysis of the results and led the writing of the manuscript. AD and GG designed the Lagrangian experiment and collected the in situ data together with FD. AP, SB and FdO provided land support concerning the sampling strategy. LI carried out the analysis of flow cytometry data. YZ provided her expertise about the flow cytometry analysis and the results obtained with the size-structured population model. All the authors discussed the results and contributed to the writing of the manuscript.

Competing interests. The contact author has declared that neither they nor their co-authors have any competing interests.

Acknowledgements. This work was supported by the CNES in the framework of the BIOSWOT-AdAC project (https://www.swot-adac.org/, last access: September 27, 2022) by the MIO Axes Transverses program (AT-COUPLAGE) and the Sino-French IRP (CNRS-CAS) DYF2M program. The chlorophyll a product is produced by CLS. The authors thank the SHOM and the crew of the RV *Beautemps-Beaupré* for shipboard operations. The authors thank also Melilotus Thyssen for providing the CytoBuoy® flow cytometer and her help in flow cytometry data analysis. The flow cytometer was funded by the CHROME project, Excellence Initiative of Aix-Marseille University – A*MIDEX, a French 11 Investissements d'Avenir program. SPASSO is operated and developed with the support of the SIP (Service Informatique de Pythéas) and in particular Christophe Yohia, Julien Lecubin, Didier Zevaco and Cyrille Blanpain (Institut Pythéas, Marseille, France). The project leading to this publication received funding from the European FEDER Fund under project number 1166-39417. Roxane Tzortzis is financed by a MENRT PhD grant (École Doctorale Sciences de l'environnement – ED 251, Aix-Marseille University).

https://doi.org/10.5194/egusphere-2022-1008
Preprint. Discussion started: 10 October 2022
© Author(s) 2022. CC BY 4.0 License.

References

Bates, A. E., Helmuth, B., Burrows, M. T., Duncan, M. I., Garrabou, J., Guy-Haim, T., Lima, F., Queiros, A. M., Seabra, R., Marsh, R., Belmaker, J., Bensoussan, N., Dong, Y., Mazaris, A. B., Smale, D., Wahl, M., and Rilov, G.: Biologists ignore ocean weather at their peril, Nature, 560, 299–301, https://doi.org/10.1038/d41586-018-05869-5, 2018.

Bethoux, J.: Oxygen consumption, new production, vertical advection and environmental evolution in the Mediterranean Sea, Deep-Sea Res., 36, 769–781, https://doi.org/10.1016/0198-0149(89)90150-7, 1989.

Cerino, F., Aubry, F. B., Coppola, J., La Ferla, R., Maimone, G., Socal, G., and Totti, C.: Spatial and temporal variability of pico-, nano-and microphytoplankton in the offshore waters of the southern Adriatic Sea (Mediterranean Sea), Cont. Shelf Res., 44, 94–105, https://doi.org/10.1016/j.csr.2011.06.006, 2012.

Claustre, H., Kerhervé, P., Marty, J. C., Prieur, L., Videau, C., and Hecq, J.-H.: Phytoplankton dynamics associated with a geostrophic front: ecological and biogeochemical implications, J. Mar. Res., 52, 711–742, https://doi.org/10.1357/0022240943077000, 1994.

Clayton, S., Nagai, T., and Follows, M. J.: Fine scale phytoplankton community structure across the Kuroshio Front, J. Plankton. Res., 36, 1017–1030, https://doi.org/10.1093/plankt/fbu020, 2014.

Cullen, J. J., Geider, R., Ishizaka, J., Kiefer, D., Marra, J., Sakshaug, E., and Raven, J.: Towards a general description of phytoplankton growth for biogeochemical models, in: Towards a model of ocean biogeochemical processes, pp. 153–176, Springer, Berlin, Heidelberg, https://doi.org/10.1007/978-3-642-84602-1_7, 1993.

De La Rocha, C. L. and Passow, U.: Factors influencing the sinking of POC and the efficiency of the biological carbon pump, Deep-Sea Res. Pt. II, 54, 639–658, https://doi.org/10.1016/j.dsr2.2007.01.004, 2007.

Dubelaar, G. B. and Jonker, R. R.: Flow cytometry as a tool for the study of phytoplankton, Sci. Mar., 64, 135–156, https://doi.org/10.3989/scimar.2000.64n2135, 2000.

Dugenne, M., Thyssen, M., Nerini, D., Mante, C., Poggiale, J.-C., Garcia, N., Garcia, F., and Grégori, G. J.: Consequence of a sudden wind event on the dynamics of a coastal phytoplankton community: an insight into specific population growth rates using a single cell high frequency approach, Front. Microbiol., 5, 485, https://doi.org/10.3389/fmicb.2014.00485, 2014.

Dumas, F.: PROTEVSMED_SWOT_2018_LEG1 cruise, RV Beautemps-Beaupré, https://doi.org/10.17183/protevsmed_swot_2018_leg1, 2018.

Edwards, K. F., Thomas, M. K., Klausmeier, C. A., and Litchman, E.: Light and growth in marine phytoplankton: allometric, taxonomic, and environmental variation, Limnol. Oceanogr., 60, 540–552, https://doi.org/10.1002/lno.10033, 2015.

Field, C. B., Behrenfeld, M. J., Randerson, J. T., and Falkowski, P.: Primary production of the biosphere: integrating terrestrial and oceanic components, Science, 281, 237–240, https://doi.org/10.1126/science.281.5374.237, 1998.

Fontana, S., Thomas, M. K., Moldoveanu, M., Spaak, P., and Pomati, F.: Individual-level trait diversity predicts phytoplankton community properties better than species richness or evenness, The ISME journal, 12, 356–366, https://doi.org/10.1038/ismej.2017.160, 2018.

Garreau, P., Dumas, F., Louazel, S., Correard, S., Fercocq, S., Le Menn, M., Serpette, A., Garnier, V., Stegner, A., Le Vu, B., et al.: PROTEVS-MED field experiments: very high resolution hydrographic surveys in the Western Mediterranean Sea, Earth. Syst. Sci. Data, 12, 441–456, https://doi.org/10.5194/essd-12-441-2020, 2020.

Hashihama, F., Saito, H., Kodama, T., Yasui-Tamura, S., Kanda, J., Tanita, I., Ogawa, H., Woodward, E. M. S., Boyd, P. W., and Furuya, K.: Cross-basin differences in the nutrient assimilation characteristics of induced phytoplankton blooms in the subtropical Pacific waters, Biogeosciences, 18, 897–915, https://doi.org/10.5194/bg-18-897-2021, 2021.

https://doi.org/10.5194/egusphere-2022-1008
Preprint. Discussion started: 10 October 2022
© Author(s) 2022. CC BY 4.0 License.

Hunter-Cevera, K. R., Neubert, M. G., Solow, A. R., Olson, R. J., Shalapyonok, A., and Sosik, H. M.: Diel size distributions reveal seasonal growth dynamics of a coastal phytoplankter, P. Natl. Acad. Sci. USA, 111, 9852–9857, https://doi.org/10.1073/pnas.1321421111, 2014.

Jacquet, S., Prieur, L., Nival, P., and Vaulot, D.: Structure and variability of the microbial community associated to the Alboran Sea frontal system (Western Mediterranean) in winter, J. Oceanogr., Research and data, 3, 47–75, https://hal.inrae.fr/hal-02656403, 2010.

Kiørboe, T.: Turbulence, phytoplankton cell size, and the structure of pelagic food webs, in: Adv. Mar. Biol., vol. 29, pp. 1–72, Elsevier, https://doi.org/10.1016/S0065-2881(08)60129-7, 1993.

Lévy, M., Klein, P., and Treguier, A.-M.: Impact of sub-mesoscale physics on production and subduction of phytoplankton in an oligotrophic regime, J. Mar. Res., 59, 535–565, https://doi.org/10.1357/002224001762842181, 2001.

Lévy, M., Franks, P., and Smith, K.: The role of submesoscale currents in structuring marine ecosystems, Nat. Commun., 9, 4758, https://doi.org/10.1038/s41467-018-07059-3, 2018.

Mahadevan, A.: The impact of submesoscale physics on primary productivity of plankton, Annu. Rev. Mar. Sci., 8, 161–184, https://doi.org/10.1146/annurev-marine-010814-015912, 2016.

Marañón, E.: Cell size as a key determinant of phytoplankton metabolism and community structure, Annu. Rev. Mar. Sci., 7, 241–264, https://doi.org/10.1146/annurev-marine-010814-015955, 2015.

Marañón, E., Cermeno, P., Latasa, M., and Tadonléké, R. D.: Temperature, resources, and phytoplankton size structure in the ocean, Limnol.Oceanogr., 57, 1266–1278, https://doi.org/10.4319/lo.2012.57.5.1266, 2012.

Marrec, P., Grégori, G., Doglioli, A. M., Dugenne, M., Della Penna, A., Bhairy, N., Cariou, T., Hélias Nunige, S., Lahbib, S., Rougier, G., Wagener, T., and Thyssen, M.: Coupling physics and biogeochemistry thanks to high-resolution observations of the phytoplankton community structure in the northwestern Mediterranean Sea, Biogeosciences, 15, 1579–1606, https://doi.org/10.5194/bg-15-1579-2018, 2018.

McDougall, T., Jackett, D., Millero, F., Pawlowicz, R., and Barker, P.: A global algorithm for estimating Absolute Salinity., Ocean Sci., 8, 1123–1134, https://doi.org/10.5194/os-8-1123-2012, 2012.

Mena, C., Reglero, P., Ferriol, P., Torres, A. P., Aparicio-González, A., Balbín, R., Santiago, R., Moyà, G., Alemany, F., and Agawin, N. S.: Prokaryotic picoplankton spatial distribution during summer in a haline front in the Balearic Sea, Western Mediterranean, Hydrobiologia, 779, 243–257, https://doi.org/10.1007/s10750-016-2825-4, 2016.

Pascual, A., Ruiz, S., Olita, A., Troupin, C., Claret, M., Casas, B., Mourre, B., Poulain, P.-M., Tovar-Sanchez, A., Capet, A., et al.: A multiplatform experiment to unravel meso-and submesoscale processes in an intense front (AlborEx), Front. Mar. Sci., 4, 39, https://doi.org/10.3389/fmars.2017.00039, 2017.

Petrenko, A. A., Doglioli, A. M., Nencioli, F., Kersalé, M., Hu, Z., and d'Ovidio, F.: A review of the LATEX project: mesoscale to submesoscale processes in a coastal environment, Ocean Dynam., 67, 513–533, https://doi.org/10.1007/s10236-017-1040-9, 2017.

Pidcock, R. E., Martin, A. P., Painter, S. C., Allen, J. T., Srokosz, M. A., Forryan, A., Stinchcombe, M., and Smeed, D. A.: Quantifying mesoscale-driven nitrate supply: A case study, Global Biogeochem. Cy., 30, 1206–1223, https://doi.org/10.1002/2016GB005383, 2016.

Qasim, S., Bhattathiri, P., and Devassy, V.: The influence of salinity on the rate of photosynthesis and abundance of some tropical phytoplankton, Mar. Biol., 12, 200–206, https://doi.org/10.1007/BF00346767, 1972.

Reynolds, C. S.: The ecology of phytoplankton, Cambridge University Press, 2006.

Ribalet, F., Marchetti, A., Hubbard, K. A., Brown, K., Durkin, C. A., Morales, R., Robert, M., Swalwell, J. E., Tortell, P. D., and Armbrust, E. V.: Unveiling a phytoplankton hotspot at a narrow boundary between coastal and offshore waters, Proc. Nat. Acad. Sci. USA, 107, 16 571–16 576, https://doi.org/10.1073/pnas.1005638107, 2010.

https://doi.org/10.5194/egusphere-2022-1008
Preprint. Discussion started: 10 October 2022
© Author(s) 2022. CC BY 4.0 License.

Rudnick, D. L.: Intensive surveys of the Azores Front: 2. Inferring the geostrophic and vertical velocity fields, J. Geophys. Res.-Oceans, 101, 16 291–16 303, https://doi.org/10.1029/96JC01144, 1996.

Schroeder, K., Gasparini, G., Borghini, M., Cerrati, G., and Delfanti, R.: Biogeochemical tracers and fluxes in the Western Mediterranean Sea, spring 2005, J. Marine Syst., 80, 8–24, https://doi.org/10.1016/j.jmarsys.2009.08.002, 2010.

Shcherbina, A. Y., Sundermeyer, M. A., Kunze, E., D'Asaro, E., Badin, G., Birch, D., Brunner-Suzuki, A.-M. E., Callies, J., Kuebel Cervantes, B. T., Claret, M., et al.: The LatMix summer campaign: Submesoscale stirring in the upper ocean, Bull. Amer. Meteorol. Soc., 96, 1257–1279, https://doi.org/10.1175/BAMS-D-14-00015.1, 2015.

Sieburth, J. M., Smetacek, V., and Lenz, J.: Pelagic ecosystem structure: Heterotrophic compartments of the plankton and their relationship to plankton size fractions, Limnol. Oceanogr., 23, 1256–1263, https://doi.org/10.4319/lo.1978.23.6.1256, 1978.

Siokou-Frangou, I., Christaki, U., Mazzocchi, M. G., Montresor, M., Ribera d'Alcalá, M., Vaqué, D., and Zingone, A.: Plankton in the open Mediterranean Sea: a review, Biogeosciences, 7, 1543–1586, https://doi.org/10.5194/bg-7-1543-2010, 2010.

Sosik, H. M., Olson, R. J., Neubert, M. G., Shalapyonok, A., and Solow, A. R.: Growth rates of coastal phytoplankton from time-series measurements with a submersible flow cytometer, Limnol. Oceanogr., 48, 1756–1765, https://doi.org/10.4319/lo.2003.48.5.1756, 2003.

Talmy, D., Blackford, J., Hardman-Mountford, N., Polimene, L., Follows, M., and Geider, R.: Flexible C: N ratio enhances metabolism of large phytoplankton when resource supply is intermittent, Biogeosciences, 11, 4881–4895, https://doi.org/10.5194/bg-11-4881-2014, 2014.

Thyssen, M., Tarran, G. A., Zubkov, M. V., Holland, R. J., Grégori, G., Burkill, P. H., and Denis, M.: The emergence of automated high-frequency flow cytometry: revealing temporal and spatial phytoplankton variability, J. Plankton Res., 30, 333–343, https://doi.org/10.1093/plankt/fbn005, 2008.

Tzortzis, R., Doglioli, A. M., Barrillon, S., Petrenko, A. A., d'Ovidio, F., Izard, L., Thyssen, M., Pascual, A., Barceló-Llull, B., Cyr, F., Tedetti, M., Bhairy, N., Garreau, P., Dumas, F., and Gregori, G.: Impact of moderately energetic fine-scale dynamics on the phytoplankton community structure in the western Mediterranean Sea, Biogeosciences, 18, 6455–6477, https://doi.org/10.5194/bg-18-6455-2021, 2021.

Worden, A. Z. and Binder, B. J.: Application of dilution experiments for measuring growth and mortality rates among Prochlorococcus and Synechococcus populations in oligotrophic environments, Aquat. Microb. Ecol., 30, 159–174, https://doi.org/10.3354/ame030159, 2003.

Zhang, Y., Jiao, N., and Hong, N.: Comparative study of picoplankton biomass and community structure in different provinces from subarctic to subtropical oceans, Deep-Sea Res. Pt. II, 55, 1605–1614, https://doi.org/10.1016/j.dsr2.2008.04.014, 2008.

https://doi.org/10.5194/egusphere-2022-1008
Preprint. Discussion started: 10 October 2022
© Author(s) 2022. CC BY 4.0 License.

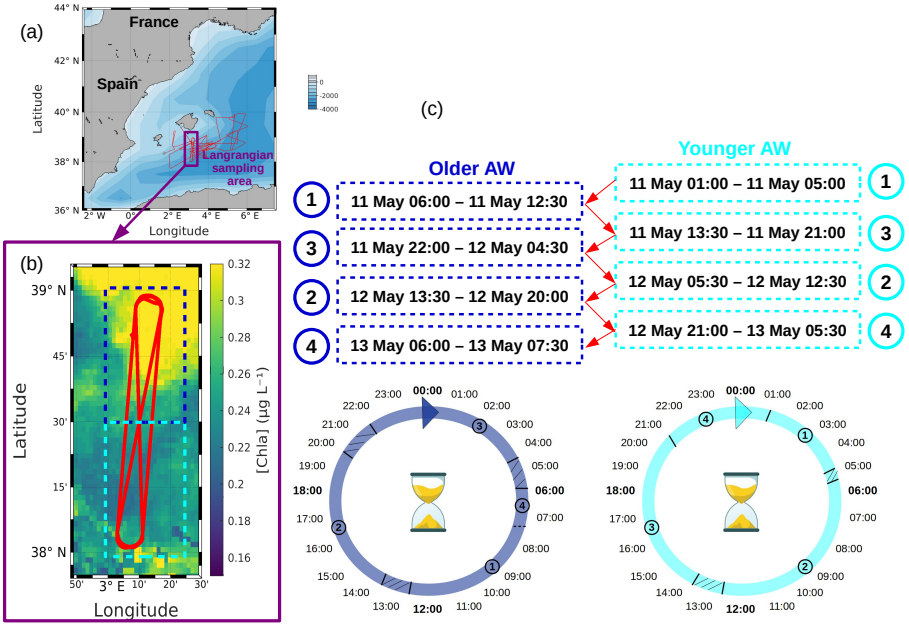

Figure 1. (a) Route of the RV *Beautemps-Beaupré* during the PROTEVSMED-SWOT cruise. The box in purple represents the area where we performed a Lagrangian strategy. (b) Map of [chla] of the 11 May 2018 superimposed on the route of the Lagrangian sampling across the older AW (in dark blue) and the younger AW (in light blue). (c) Dates of the transects across the older AW and the younger AW, used to reconstruct a day of 24 h period in each water mass.

https://doi.org/10.5194/egusphere-2022-1008
Preprint. Discussion started: 10 October 2022
© Author(s) 2022. CC BY 4.0 License.

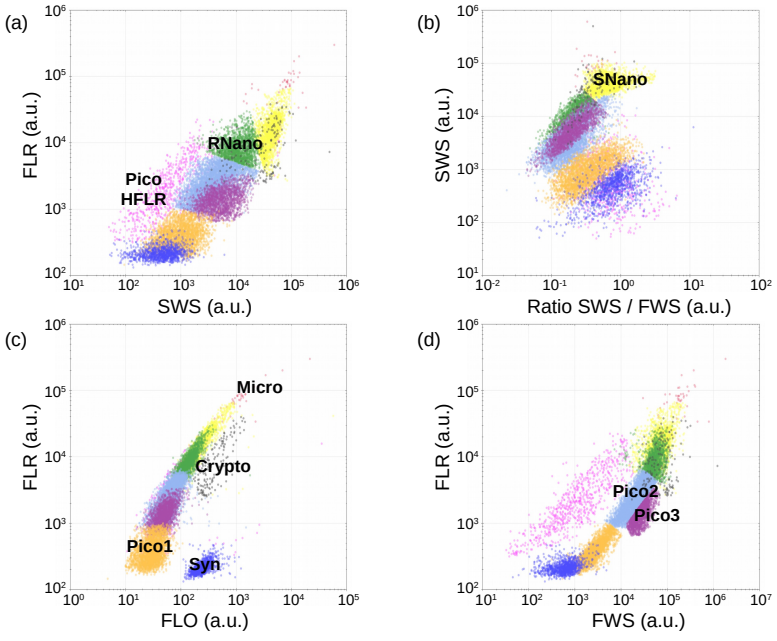

Figure 2. Cytograms obtained with the CytoSense automated flow cytometer. *Synechococcus* are in dark blue (Syn), the picophytoplankton with lowest FLO in orange (Pico1), the picophytoplankton with intermediate FWS in light blue (Pico2), the picophytoplankton with highest FWS in purple (Pico3), the picophytoplankton with a high red fluorescence in pink (PicoHFLR), the nanophytoplankton with high SWS/FWS ratio in yellow (SNano) and higher SWS intensities than the other nanophytoplankton (RNano) in green, the Cryptophytes in grey (Crypto) and the microphytoplankton in red (Micro). The flow cytometry units for both fluorescence and light scatter are arbitrary (a.u). Figure extracted from Tzortzis et al. (2021).

https://doi.org/10.5194/egusphere-2022-1008
Preprint. Discussion started: 10 October 2022
© Author(s) 2022. CC BY 4.0 License.

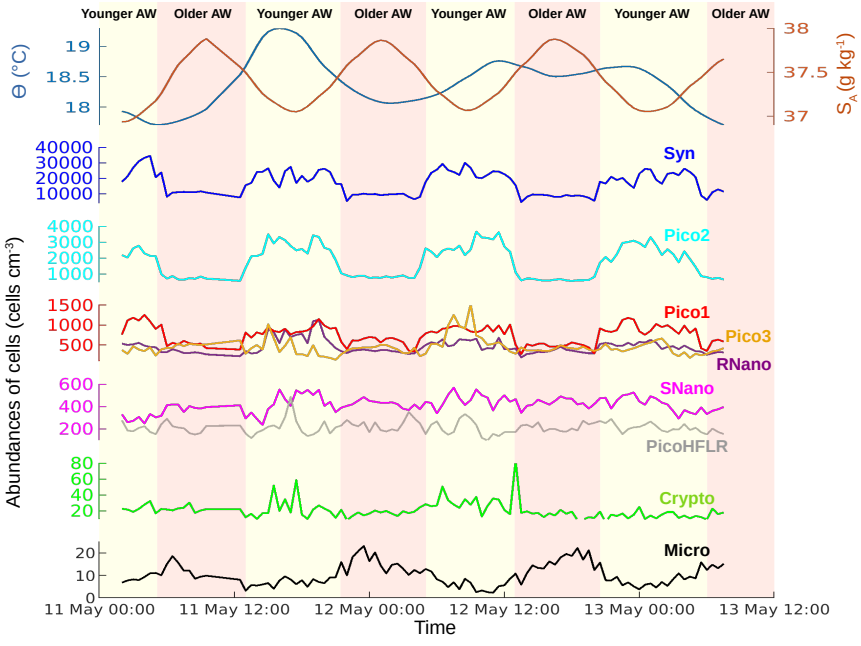

Figure 3. Temporal evolution of sea surface conservative temperature (Θ) in °C, absolute salinity (S_A) in $\mathrm{g\,kg^{-1}}$, and phytoplankton abundances in $\mathrm{cells\,cm^{-3}}$, from 11 May 00:00 to 13 May 12:00 (UTC). Vertical colors correspond to the two water masses separated by the front (see Fig. 1).

https://doi.org/10.5194/egusphere-2022-1008
Preprint. Discussion started: 10 October 2022
© Author(s) 2022. CC BY 4.0 License.

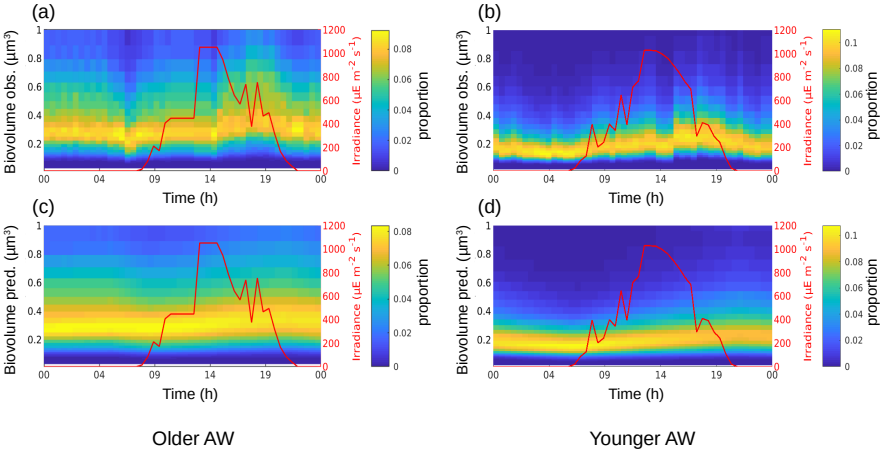

Figure 4. Observed (a, b) and predicted (c, d) hourly normalized cell size distribution, i.e., biovolume (μm^3) for *Synechococcus* in the older AW (a, c) and the younger AW (b, d), superimposed with the irradiance ($\mu E\, m^{-2}\, s^{-1}$).

https://doi.org/10.5194/egusphere-2022-1008
Preprint. Discussion started: 10 October 2022
© Author(s) 2022. CC BY 4.0 License.

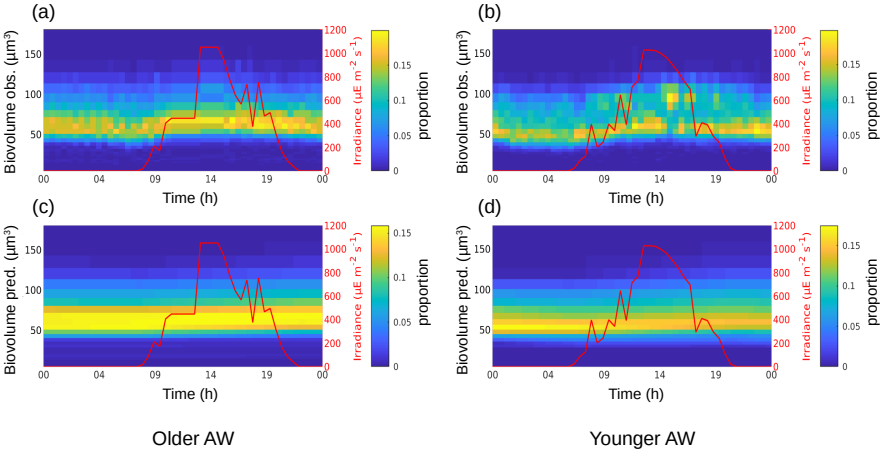

Figure 5. Observed (a, b) and predicted (c, d) hourly normalized cell size distribution, i.e., biovolume (μm^3) for RNano in the older AW (a, c) and the younger AW (b, d), superimposed with the irradiance ($\mu E\, m^{-2}\, s^{-1}$).

https://doi.org/10.5194/egusphere-2022-1008
Preprint. Discussion started: 10 October 2022
© Author(s) 2022. CC BY 4.0 License.

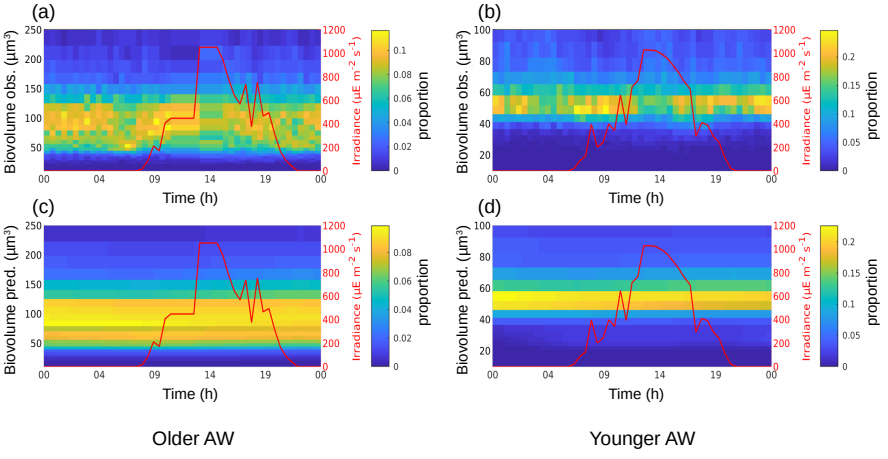

Figure 6. Observed (a, b) and predicted (c, d) hourly normalized cell size distribution, i.e., biovolume (μm^3) for SNano in the older AW (a, c) and the younger AW (b, d), superimposed with the irradiance ($\mu E\, m^{-2}\, s^{-1}$).

https://doi.org/10.5194/egusphere-2022-1008
Preprint. Discussion started: 10 October 2022
© Author(s) 2022. CC BY 4.0 License.

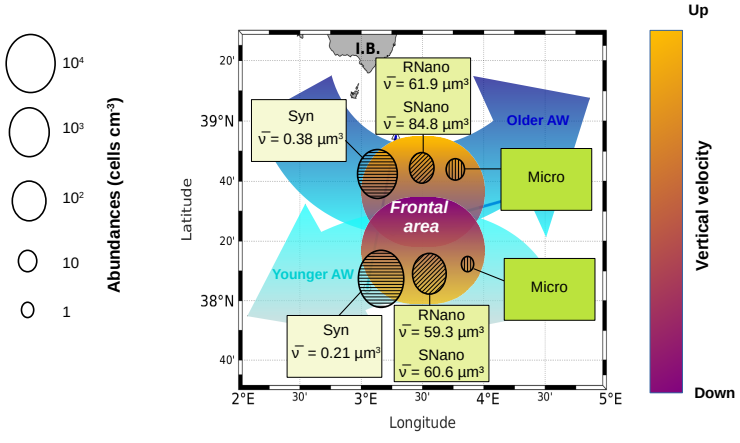

Figure 7. Distribution of phytoplankton biovolumes and abundances in the frontal area. Figure adapted from Tzortzis et al. (2021).

https://doi.org/10.5194/egusphere-2022-1008
Preprint. Discussion started: 10 October 2022
© Author(s) 2022. CC BY 4.0 License.

Table 1. Model parameters.

Parameters	Definition	Interval	Units
dt	Time step	$\frac{10}{60}$	hours
γ_{max}	Max proportions of cells in growing phase	[0,1]	$\emptyset$
E^*	Irradiance scaling	[0,∞[	$\mu\mathrm{E}\,\mathrm{m}^{-2}\,\mathrm{s}^{-1}$
δ_{max}	Max proportions of cells in mitosis	[0,1]	$\emptyset$
μ_v	Mean of size density distribution	$[v_{min}, v_{max}]$	$\mu\mathrm{m}^3$
σ_v	Standard deviation of size density distribution	$[10^{-06}$,∞[	$\mu\mathrm{m}^3$
μ_t	Mean of temporal density distribution	$[1,24\frac{1}{dt}+1]$	hours
σ_t	Standard deviation of temporal density distribution	$[10^{-06}$,∞[	hours

https://doi.org/10.5194/egusphere-2022-1008
Preprint. Discussion started: 10 October 2022
© Author(s) 2022. CC BY 4.0 License.

Table 2. Means of biovolumes (v_{mean} in μm^3), growth rates (μ_{size}, μ_{ratio} in d^{-1}) and loss rate (l in d^{-1}) values for the phytoplankton groups, in the older and younger AW. μ_{size} represents the PFG intrinsic growth rates (d^{-1}) and mean size ratio $\mu_{ratio} = ln(v_{max}/v_{min})$ was calculated to provide an indication about the model performance and the synchronicity of populations (Dugenne et al., 2014).

	Synechococcus	RNano	SNano
Older AW	v_{mean} = 0.38 ± 0.27	v_{mean} = 61.9 ± 20.6	v_{mean} = 84.8 ± 43.4
	μ_{size} = 0.25 ± 0.91	μ_{size} = 0.01 ± 0.00	μ_{size} = 0.04 ± 0.26
	μ_{ratio} = 0.59	μ_{ratio} = 0.17	μ_{ratio} = 0.11
	l = -0.64	l = -0.87	l = -0.32
Younger AW	v_{mean} = 0.21 ± 0.13	v_{mean} = 59.3 ± 21.2	v_{mean} = 60.6 ± 35.3
	μ_{size} = 0.71 ± 1.40	μ_{size} = 0.04 ± 0.28	μ_{size} = 0.06 ± 0.06
	μ_{ratio} = 0.63	μ_{ratio} = 0.33	μ_{ratio} = 0.24
	l = -0.21	l = -1.32	l = -0.82

https://doi.org/10.5194/egusphere-2022-1008
Preprint. Discussion started: 10 October 2022
© Author(s) 2022. CC BY 4.0 License.

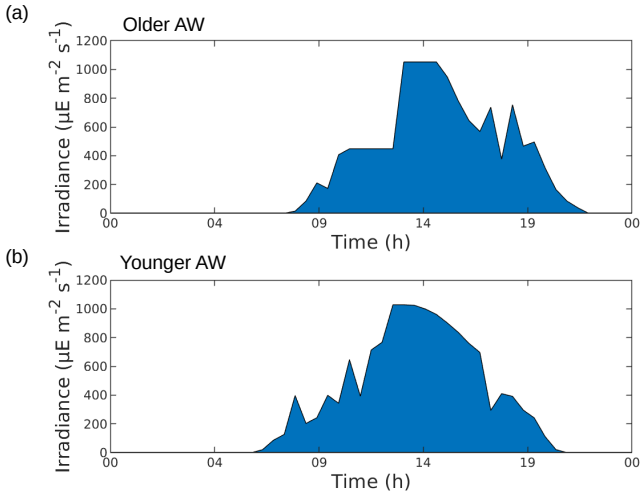

Figure A1. Reconstruction of irradiance during 24 h in the older AW (a) and the younger AW (b). Computation of trapezoidal integration of irradiance, in the older AW, E1 = 286 µE $\mathrm{m}^{-2}\,\mathrm{s}^{-1}$ and in the younger AW, E2 = 299 µE $\mathrm{m}^{-2}\,\mathrm{s}^{-1}$.

https://doi.org/10.5194/egusphere-2022-1008
Preprint. Discussion started: 10 October 2022
© Author(s) 2022. CC BY 4.0 License.

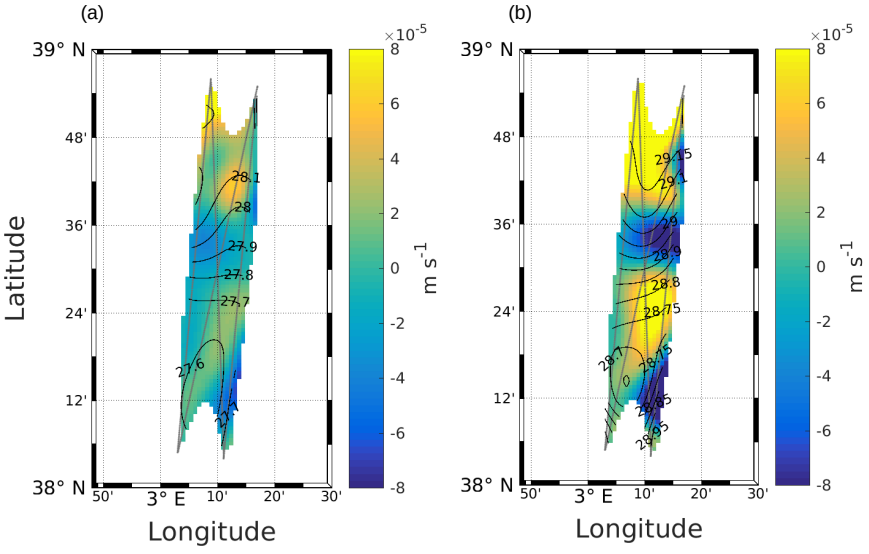

Figure A2. Vertical velocities at 25 m (a) and 85 m (b), calculated with the omega equation. Figure extracted from Tzortzis et al. (2021).